Received: 31 July 2019 | Revised: 29 May 2020 | Accepted: 3 June 2020

DOI: 10.1002/ldr.3692

WILEY

RESEARCH ARTICLE

Spatiotemporal analysis of deforestation in the Chapare region of Bolivia using LANDSAT images

Hasi Bagan[1,2] | Andrew Millington[3] | Wataru Takeuchi[4] | Yoshiki Yamagata[2]

[1]School of Environmental and Geographical Sciences, Shanghai Normal University, Shanghai, PR, China

[2]Center for Global Environmental Research, National Institute for Environmental Studies, Ibaraki, Japan

[3]College of Science and Engineering, Flinders University, Adelaide, South Australia, Australia

[4]Institute of Industrial Science, The University of Tokyo, Tokyo, Japan

Correspondence
Hasi Bagan, School of Environmental and Geographical Sciences, Shanghai Normal University, Shanghai 200234, PR, China.
Email: hasi.bagan@nies.go.jp

Funding information
National Natural Science Foundation of China, Grant/Award Number: 41771372; UK National Environmental Research Council; EU Framework IV; Texas Agricultural Experiment Station; Flinders University

Abstract

The purpose of this study is to quantify (a) spatiotemporal deforestation patterns, and (b) the relationships between changes in the main land-cover types in the Chapare region of Bolivia. We applied subspace classification methods to LANDSAT data from 1986, 1999, and 2018 and used grid cells at scales of 150, 300, 600, and 900 m to measure deforestation trajectories. The 150 m grids provided better detail to determine deforestation trajectories than coarser-scale grid cells. Differences in grid-cell scale did not influence the statistical trends in land-cover changes significantly. Changes in forest area were negatively correlated with changes in cropland (r = −.44), grassland (r = −.34), swamp grassland (r = −.38), and regrowth (r = −.32) areas. Correlations between forest losses in cropland, grassland, and regrowth change analyses were weaker between 1999 and 2018 compared to 1986 to 1999. Forest cover declined from 6,635 km^2 (1986) to 3,800 km^2 (2018), and the deforestation rate increased from an annual average of 1.36% between 1986 and 1999 to 2.0% between 1999 and 2018. The key proximate drivers of forest clearance rates and patterns were increasing population, agricultural expansion, and road building. While coca is an economically important crop in Chapare, its direct and indirect effects on deforestation could not be determined unambiguously. It is probable that the expansion of agriculture will lead to further deforestation and forest fragmentation and, along with decreases in forest cover, further changes will take place between non-forest categories.

KEYWORDS

Amazon Basin, Chapare, coca cultivation, deforestation, grid-cell analysis, LANDSAT, spatiotemporal analysis

1 | INTRODUCTION

The forests of the Amazon Basin play important roles in carbon sequestration, biodiversity conservation, moisture recycling, and atmospheric circulation at local, regional, and global scales (Lima et al., 2014; Marengo et al., 2018; Ometto, Aguiar, & Martinelli, 2011; Tejada et al., 2016). Consequently, accurate accounting of changes in forest cover are essential for understanding and mitigating the impacts of climate change, and are a key requirement for managing ecosystem services (Bovolo & Donoghue, 2017; Grinand et al., 2013).

This research focuses on the southwestern Amazon Basin, specifically the Chapare region in the lowlands of Cochabamba Department in Bolivia. Historically, terrestrial vegetation in Chapare was dominated by humid tropical forests which exhibited ecological variation due to topographic and hydrologic conditions (Godoy, Morduch, & Bravo, 1998; Paneque-Gálvez et al., 2018). It was very lightly used by nomadic Amerindian tribal groups (Rodríguez Ostria, 1972) prior to being transformed by farmers who began to migrate to the region in the early 20th Century.

From the late 1950s and early 1960s migration rates increased as the Bolivian Government actively promoted colonization in Chapare

by establishing permanent settlements, providing farm plots with legal tenure, and building roads to attract migrants from elsewhere in the country (Bradley & Millington, 2008a; Godoy et al., 1998; Henkel, 1995; Millington, 2018; Millington, Velez-Liendo, & Bradley, 2003; Müller, Pacheco, & Montero, 2014; van Gils & Ugon, 2006). Little original forest now remains due to clearance which has created a fine-grained mosaic of banana, citrus, palm, and rubber plantations; pineapple, manioc, rice, and coca fields; pastures; and secondary forest regrowth (Delgado, 2017).

This land-use mosaic is the result of complex interactions between deforestation drivers such as selective logging for timber; forest clearance for coca cultivation, and crops that have been promoted as alternatives to coca; cattle rearing; and infrastructure development. Settlement in the late 1950s and 1960s led to an expansion of agriculture in central Chapare (Millington, 2018). The increase in coca cultivation, associated with the global increase in cocaine use in the 1970s (Delgado, 2017), stimulated further forest clearance (Killeen et al., 2008) as farmers began to clear old-growth forests in southeastern Chapare (Millington et al., 2003; Dávalos et al., 2011).

Bolivia has alternated between being the second- or third-highest coca-producing country globally since the 1970s. Illicit coca cultivation in Bolivia is defined in law by the Bolivian Government. Most illicit coca is grown in Chapare and a very large proportion ends up in the cocaine trade (UNODC, 2019). These facts underpin the need to acknowledge the role of coca in understanding deforestation in Chapare. It also makes it different to most other deforested areas in the Amazon Basin, with the exception of a few lowland coca-producing areas in Colombia and Peru.

The role of coca in deforestation is confounded by the fact that, unlike most other crops, it is a high-yielding cash crop that requires low inputs (Grimmelmann, Espinoza, Arnold, & Arning, 2017; Henkel, 1995) and relatively little land (Bradley & Millington, 2008a; Kaimowitz, 1997). Therefore, the direct effects of clearing forest to create coca fields on deforestation rates is probably much less than the larger indirect impact on forest clearance (Hoffmann, Márquez, & Krueger, 2018). Grisaffi and Ledebur (2016) argue that attempts to control coca through eradication and planting alternative crops have accentuated the diversity of the cropland, plantation, forest clearance, and regrowth mosaic that characterizes the Chapare.

Issues associated with coca and land use are confounded by the scarcity of accurate statistics on coca cultivation prior to the establishment of the United Nations Office for Drug Control (UNODC) coca monitoring system for Bolivia in 2004; which has subsequently produced annual reports (see UNODC, 2019, for latest report). According to Henkel (1995) coca cultivation increased from approximately 15,000 to 61,000 ha between 1978 and 1990, while Millington (2018) shows that coca leaf production in Chapare increased from 11,800 to 36,000 t between 1974 and 1990.

How the direct and indirect effects of all of these drivers have played out across Chapare is unclear and there is a pressing need for spatiotemporal quantitative analysis of forest loss; not least so that effective biodiversity conservation strategies, ecosystem preservation, and rural development activities can be designed and implemented (Paneque-Gálvez et al., 2013).

Understanding the potentially scale-dependent, spatiotemporal variability in deforestation in Chapare is a further challenge. Many studies have sought to identify the spatial and temporal dynamics of forest-cover change in the Amazon (Bottazzi & Dao, 2013; Hansen et al., 2013; Malingreau, Eva, & De Miranda, 2012; Pinto-Ledezma & Mamani, 2014; Tyukavina et al., 2017). However, a lack of relevant multitemporal, land-cover maps has limited these efforts because many land-cover datasets are only available from 2000 or have relatively low spatial resolutions. Both longer time frames and fine-spatial resolution data are necessary to capture environmental and socioeconomic variability at fine-spatial resolutions when analyzing land-cover change.

Consequently, the focus of this study is on the use of Landsat data and GIS techniques to quantify spatiotemporal patterns of forest-cover change in Chapare from 1986 to 2018. We used subspace classification to accurately classify land cover using Landsat images acquired in 1986, 1999, and 2018. It is difficult to (a) visualize spatiotemporal patterns of forest change, and (b) quantify relationships between land-cover classes change from the pixel-based transition matrices generated by many image classification algorithms. The overcome this a grid-cell methodology was used as an alternative way to investigate relationships between changes in land-cover classes. Therefore, its application has direct relevance to improving our understanding of the relationships between the growing demand for agricultural land and future deforestation trends, and in understanding direct and indirect drivers of deforestation.

2 | MATERIALS

2.1 | Study area

The Chapare region we report on covers approximately 9,500 km^2. It is located in the southwestern Amazon Basin and is centered on 16.50°S, 65.00°W (Figure 1a; Grisaffi & Ledebur, 2016). Chapare, as used in this article, refers to the study area and not the Bolivian administrative unit called Chapare Province. It is based on one of the main areas in Bolivia surveyed annually by the UNODC to monitor coca cultivation. Adjustments to the UNODC area reflect our understanding of the ecology and colonization of the area from fieldwork conducted since 1998. The term Chapare has routinely been used in the scientific literature to refer to this area (Bradley & Millington, 2008a; Farthing & Kohl, 2010; Grisaffi & Ledebur, 2016; Henkel, 1995; Killeen et al., 2007; Millington, 2018 and references therein). We have adopted this usage in this article, while acknowledging the confusion that arises if it is not defined. The area reported on therefore includes the lowland parts of Carrasco, Chapare, Ichilo, and Tiraque Provinces of Cochabamba Department (http://data.humdatat.org/datatset/bolivia-administrative-level-0-3-boundary-polygons): the highland parts of which are not relevant to this research. Consequently, our

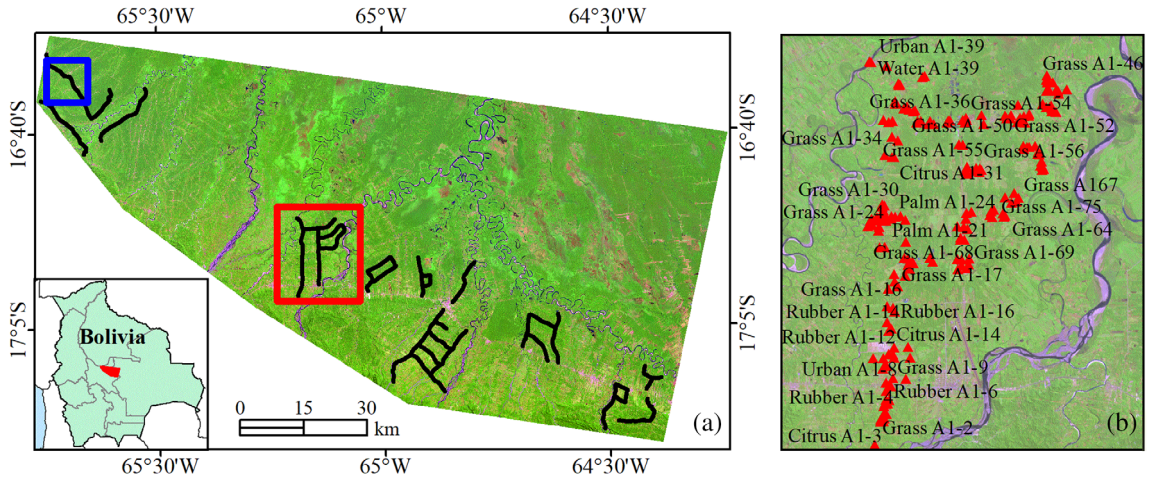

FIGURE 1 Study area (a) 2018 OLI image (RGB = bands 6, 5, 3), and (b) closer view of some fieldwork plot locations with details of land-cover information {red rectangle in (a)}. The black lines in (a) indicates the 12 transects, and the blue rectangle in (a) indicates the area covered by the images in Figure 7 and Figure S3. OLI, Operational Land Imager [Colour figure can be viewed at wileyonlinelibrary.com]

research findings apply to the lowlands of all four of these provinces.

The area is located adjacent to the Andes. Large rivers that drain the Andes to the south traverse the region before joining the Mamoré River, a major tributary of the Amazon River. The area forms an ecotone extending from the forested foothills of the Andes in the south to swamps and seasonally flooded grasslands and forests in the north. The lowland areas adjacent to the foothills are not subject to regular seasonal flooding as they comprise alluvial fans which reach elevations of around 300 m.a.s.l.. Mean annual rainfall ranges from 2,500 to 7,000 mm, with most falling between October and March (Killeen et al., 2007; Montes de Oca, 1997).

2.2 | Satellite imagery and field verification data

Free, open-access LANDSAT imagery are highly suited to the detection of land-cover change (Wulder et al., 2019) in agricultural regions (Yin et al., 2018), urban areas (Awotwi, Anornu, Quaye-Ballard, & Annor, 2018), grasslands (Batunacun, Hu, & & Lakes, 2018), and when analyzing forest-cover dynamics (Achard et al., 2014; Hansen et al., 2013; Keenan et al., 2015; Lu, Batistella, Mausel, & Moran, 2007). Moreover, LANDSAT images are ideal for identifying and characterizing the spatial and temporal relationships between forest-cover change and other anthropogenic land-cover changes (Bagan & Yamagata, 2014; Duveiller, Defourny, Desclée, & Mayaux, 2008). We acquired LANDSAT Thematic Mapper (TM), Enhanced Thematic Mapper plus (ETM+), and Operational Land Imager (OLI) Level-1TP data for the study area for 1986, 1999, and 2018 from the US Geological Survey (Table 1). These years were selected for the following reasons:

1. 1986 was the year with the earliest available cloud-free TM imagery during the 1970s–1980s 'coca boom';
2. in 1999 the area planted to coca was very low after successful eradication programs during the 1990s; and
3. coca cultivation began to increase again with the growing influence of the MAS (Movement to Socialism) Party and the election of Morales-led governments from 2005 to 2019. Therefore, 2018 reflects 18 years of pro-coca policies that were integral to broader land, agrarian, and social reforms in Bolivia (Farthing & Kohl, 2010; Grisaffi & Ledebur, 2016; Kohl & Breshahan, 2010; Morales, 2013).

TABLE 1 Acquisition dates for the LANDSAT imagery used

Satellite-sensor	Acquisition date	Path/row
LANDSAT 5 TM	October 4, 1986	232/072
LANDSAT 7 ETM+	July 12, 1999	232/072
LANDSAT 8 OLI	September 10, 2018	232/072

Abbreviations: ETM+, Enhanced Thematic Mapper Plus; OLI, Operational Land Imager; TM, Thematic Mapper.

Cloud-free images were acquired between July and October (the dry season), when differences in rates of photosynthesis between different land-cover types are at a maximum in the region. They were preprocessed for standard terrain corrections by the US Geological Survey. All analyses were based on the optical and thermal infrared bands of the LANDSAT TM, ETM+, and OLI images: panchromatic bands were not used. We did not perform the atmospheric correction process in this study, but the atmospheric correction could be an improvement (Song, Woodcock, Seto, Lenney, & Macomber, 2001). It is worth noting that previous studies have shown that using multi-date image segmentation for classification can improve the robustness of land-cover change analysis. It helps to reduce the error caused by using land-cover images independently classified from separate remote sensing images, and can reduce the problem of error

propagation when using classified images to estimate land-cover change trajectories (Duveiller et al., 2008; Hussain, Chen, Cheng, Wei, & Stanley, 2013).

We conducted field campaigns in Chapare in August 2003 and 2007, and September 2015. A total of 450 land-use/land-cover recording sites were established along 12 transects (Figure 1a). Recording sites were established in 2003 in central and eastern Chapare, and sites in western Chapare were added in 2007. When the sites were first established we aimed for approximately equal numbers of primary forest; low, medium and high secondary regrowth; swamp forest and grassland; field crops; tree crop plantations; grassland/pasture; bare soil; urban fabric and road-land parcels. Once a relatively large area of a particular land cover was located, a sketch map of the site with all the land parcels within approximately 250 m in all directions from a recording point was drawn. A GPS reading was made at the recording point. Subsequent land-use changes in the region have led to changes in the proportions of each land-cover class at the 450 sites. In addition, the number of land-cover parcels has changed, mainly due to conversion of natural vegetation to small fields, and the merging and splitting of fields. In the 2015 survey, records were

TABLE 2 Description of land-cover types and the number of training and validation samples for images acquired in 1986, 1999, and 2018

		1986		1999		2018	
Class name	Class description	Training	Validation	Training	Validation	Training	Validation
C1. Water	Permanent water bodies, rivers, lakes, and ponds	473	191	758	239	811	269
C2. Dense swamp grassland	Dense swamp grass, >80% cover	606	202	419	181	695	223
C3. Sparse swamp grassland	Low-density swamp grass, with open expanses of bare ground and standing water	658	221	822	239	994	223
C4. Bare ground	Covered by sand and/or gravel in dry and wet seasons	460	168	807	245	778	225
C5. Forest in shadow	Lower montane forest in shadow, mainly in the Andes foothills comprising mature trees forming a dense and structurally complex canopy with few gaps	433	201	613	222	562	202
C6. Forest, illuminated	Illuminated lower montane, mainly in the Andes foothills comprising mature trees forming a dense and structurally complex canopy with few gaps	509	206	676	206	554	204
C7. Dense lowland forest	Forested areas with low levels of disturbance that consist of mature trees forming a dense and structurally complex canopy with few gaps. It is probable that some mature secondary forest occurs in the class	893	291	985	245	606	219
C8. Lowland swamp forest	Flooded forests with varying degrees of disturbance due to natural dynamics (e.g., flooding regimes)	508	203	455	207	377	103
C9. Cropland	All agricultural fields and plantations with crops.	558	253	853	219	747	192
C10. Regrowth	Early to medium stages of forest regeneration, identified by shrub and tree height and indicator plants	282	129	794	206	604	209
C11. Sparse grassland	Cleared fields and well-grazed pastures	410	165	742	244	543	150
C12. Dense grassland	Areas dominated by dense grassland (>80% cover), often with shrub regrowth, indicating abandoned fields and pastures	447	178	965	205	410	151
C13. Medium-density grassland	Areas dominated by medium-density grassland (50–80% cover), occasionally with shrubs. Normally indicative of pastures with lover grazing density	316	174	661	238	342	161
C14. Urban/built-up	All residential, commercial and industrial areas, including transport infrastructure	498	171	636	224	992	270
Total		7,051	2,753	10,186	3,120	9,015	2,801

obtained for approximately 2,200 land parcels at the 450 sites. In addition to recording the land cover for each land parcel within the vicinity of a recording site, we also noted geomorphological, pedological and hydrological information; and took ground photographs.

We tied these sites to the image data with the field GPS readings (Figure 1b). For the research reported in this article land-cover information acquired during the field campaigns was converted into 14 land-cover classes, based on field notes and the visual interpretation of high-spatial resolution images from WorldView-2 and -3, and from Google Earth and LANDSAT composites (Table 2). Then, we generated ground reference samples across the study area and labeled them based on the information from the field survey records. These reference samples were split into two sets of samples to generate sets of training sites units and validation sample units that were spatially separate. Each sample unit contained at least nine pixels (Congalton & Green, 2008).

3 | METHODS

3.1 | Subspace classification

Subspace methods (Oja, 1983) provide a practical solution for pattern recognition in image sets (Fukui & Maki, 2015; Park & Konishi, 2019) and have been applied to remote sensing data by Bagan and Yamagata (2012). Recent studies indicate that no single classification method can fulfil all classification requirements (Abdi, 2019; Kiang, 2003). Subspace methods provide an alternative to supervised classification approaches (Bagan, Kinoshita, & Yamagata, 2012). Subspace classification was applied to each of the three datasets used in this research (Table 1). This enables us to report on the first application of subspace classification methods to a complex mosaic of humid tropical forest, cropland, pasture, and secondary regrowth. Such landscapes have proven a challenge to land-change scientists using relatively small-spatial resolution, remotely sensed data acquired from the LANDSAT series of satellites and sensors in the past.

Subspace methods transform the original data from high-dimensional to low-dimensional feature space, while preserving the discriminative properties of the different classes. This significantly reduces computational cost and leads to more feasible subspaces. Figure 2 illustrates the concept of subspace method classification.

To improve the performance and training stability of the subspace method, normalization processing is used to rescale the pixel values to the 0–1 range. In this research the image data, and training and validation pixels, were normalized as follows during preprocessing. Let d be the number of image bands. For a given pixel $x = (x_1, x_2, \ldots, x_d)^T$ that x is a column vector, the normalized pixel is computed as:

$$x = (x_1/L, x_2/L, \ldots, x_d/L)^T \quad (1)$$

where $L = \sqrt{x_1^2 + x_2^2 + \ldots + x_d^2}$ and the superscript T denotes the matrix transpose operator. Let x denote the normalized pixel for convenience.

We denote the subspace of k^{th} land-cover class by C_k, and using $\varphi_{k,i}$ ($1 \le i \le r$, $1 \le k \le K$) to denote the i^{th} basis vector in the k^{th} land-cover class, which is computed from the class-training sample data covariance matrix by eigenvalue- and eigenvector-solving algorithms. Here r is the dimensionality of the subspace C_k, and K denotes the number of land-cover classes.

Let column vectors $s_{k,i}$ ($1 \le i \le N_k$) be a set of training samples of k^{th} land-cover class, where N_k is the number of training samples belonging to k^{th} land-cover class. Then we form a matrix $S_k = [s_{k,1}, \cdots, s_{k,N_k}]$. Subsequently the covariance matrix of the subspace C_k can be evaluated as

$$Cov_k = \frac{1}{N_k - 1} S_k S_k^T \quad (2)$$

This is a multiplication of a $d \times N_k$ matrix, S_k, by a $N_k \times d$ matrix S_k^T, which results in a $d \times d$ matrix. Than we calculate the eigenvalues of Cov_k, and select the r eigenvectors $\varphi_{k,i}$ ($1 \le i \le r$, $1 \le k \le K$) corresponding to the first r largest eigenvalues (in decreasing order). These r eigenvectors are used as basis vectors to form the subspace C_k.

The basic class-featuring information compression (CLAFIC) subspace method measures the similarity between the pixel x and the k^{th} class by using the projection norm onto the subspace C_k,

$$S_k(x) = S(x, C_k) = \sum_{i=1}^{r} \left(x^T \varphi_{k,i}\right)^2 \quad (3)$$

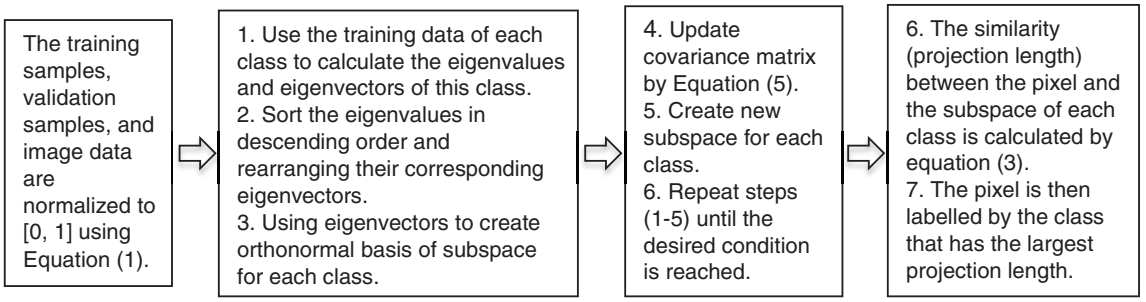

FIGURE 2 Schematic diagram of the subspace training and classification process

Consequently, the pixel x is classified into that class whose squared projection length $S_k(x)$ is maximum. To reduce misclassification in the overlapping regions of two or more class subspaces, the CLAFIC method has been modified to the averaged learning subspace method (ALSM), which adopts the iteration process and adaptively computes the subspaces to reduce classification error. In ALSM, the following solutions are used to update the class covariance matrix so that the overlap between subspaces is reduced.

At iteration t ($t > 0$), the conditional covariance matrix is calculated based on the misclassified training pixels as

$$Cov_{p,q}^{(t)} = \sum_{x} \{xx^T | x \in C_p, x \rightarrow C_q\}, p \neq q. \quad (4)$$

where the symbol "→" denotes that the training pixel x belonging to p^{th} land-cover class ($1 \le p \le K$) has been mislabeled into q^{th} land-cover class ($1 \le q \le K$).

Then, we updated the covariance matrix, which we denote by $Cov_p^{(t)}$, for p^{th} class as:

$$Cov_p^{(t)} = Cov_p^{(t-1)} + \alpha \sum_{q=1, q \neq p}^{K} Cov_{p,q}^{(t)} - \beta \sum_{q=1, q \neq p}^{K} Cov_{q,p}^{(t)} \quad (5)$$

where α and β are small positive constant values, and set the initial conditional covariance matrix to $Cov_p^{(0)} = Cov_p$. The eigenvalues and eigenvectors of $Cov_p^{(t)}$ are then calculated to generate a new subspace C_p. Repeat the iterative process until the preset maximum number of iterations is reached or the required recognition rate is reached (Bagan & Yamagata, 2010). In this study, the subspace dimensions were fixed at four for each of the images used.

3.2 | Grid-cell processing

Grid-cell processing was used in this study to investigate whether the patterns of forest clearance and correlations between changes in land-cover classes were scale dependent. The grid-cell approach represents a good compromise between necessary detail and computational feasibility (Bagan & Yamagata, 2012; Shoman, Alganci, & Demirel, 2019). For unbiased spatiotemporal analysis and to find particular spatial characteristics related to deforestation and forest fragmentation between two dates, we created nets of grid cells at scales of 150 × 150 m, 300 × 300 m, 600 × 600 m, and 900 × 900 m covering the entire study area. We used these different grid-cell scales to investigate any scale dependency in the relationships between changes in forest area and changes in other land-cover classes. Another important advantage of grid cells with unique cell identifiers is that they enable land-cover maps to be linked unambiguously when analyzing land-cover change. We explain the procedures for merging land-cover classes, and for linking grid cells and land-cover classes below.

First, we merged similar land-cover categories (Table 2) into single classes for analysis: dense and sparse swamp grassland were merged into the swamp grassland class; forest in shadow, forest (illuminated), dense lowland forest, and lowland swamp forest were merged into the forest class; and dense, medium-density, and sparse grassland were merged into the grassland class. After merging the target classes, the merged land-cover maps for 1986, 1999, and 2018 had eight land-cover types: water, swamp grassland, bare ground, forest, cropland, regrowth, grassland, and urban/built-up.

Next, we used the intersection of the 150 m grid cells with the eight-class land-cover maps to calculate the area of each land-cover class in each grid-cell, and transferred the results to new attribute fields using ArcGIS 10.6 software. Finally, we divided the area of each land-cover class by the area of the grid-cell to calculate the percentages of each grid-cell occupied by each class. We repeated the process for grid cells at 300 m, 600 m, and 900 m scales, and transferred the results, expressed as percentages of the grid-cell occupied by each class, to new attribute fields.

3.3 | Deforestation rate

We also calculated the annual standardized deforestation rate (ρ) using percentage of forest cover area (Puyravaud, 2003):

$$\rho = 100 \times \frac{1}{t_2 - t_1} \ln\left(\frac{A_2}{A_1}\right), \quad (6)$$

where ρ is the annual rate of deforestation (as a percentage), and A_1 and A_2 are the forest-cover areas in years t_1 and t_2, respectively.

4 | RESULTS

4.1 | Spatiotemporal changes of the land-cover classes

The accuracies of the subspace classifications obtained for each image were evaluated in terms of producer's accuracy and overall accuracy (Congalton & Green, 2008). The overall accuracies ranged between 75.5 and 78.4% for the 14 land-cover categories (Figure S1).

After creating the eight merged land-cover classes, the classification accuracies for the swamp grassland, forest, and grassland classes improved in that they exhibited less variability and were generally close to the highest accuracies of the individual classes that had been merged (Figure 3).

We prepared land-cover classification maps for 1986, 1999, and 2018 (Figure 4a) using the merged classes and calculated the percentage of area occupied by each class after merging (Figure 4b). The total area of agricultural land uses (grassland and cropland) increased from 7.6% of the study area in 1986 to 18.3% (1999) and 20.6% (2018), while the forest area decreased from 69.8% in 1986 to 40.0% in 2018, with an intermediate value of 58.5% in 1999 (Table 3).

FIGURE 3 Merged land-cover classification accuracies (%) for 1986, 1999, and 2018

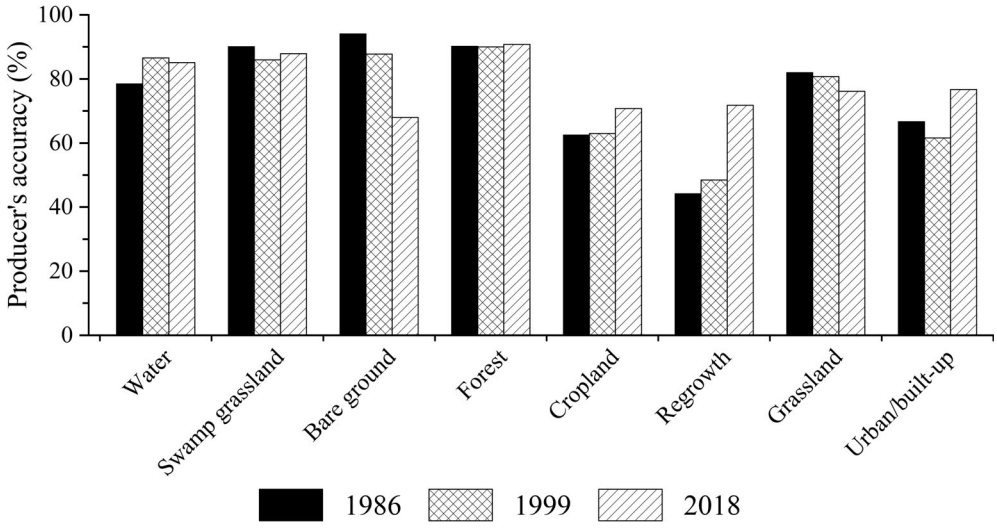

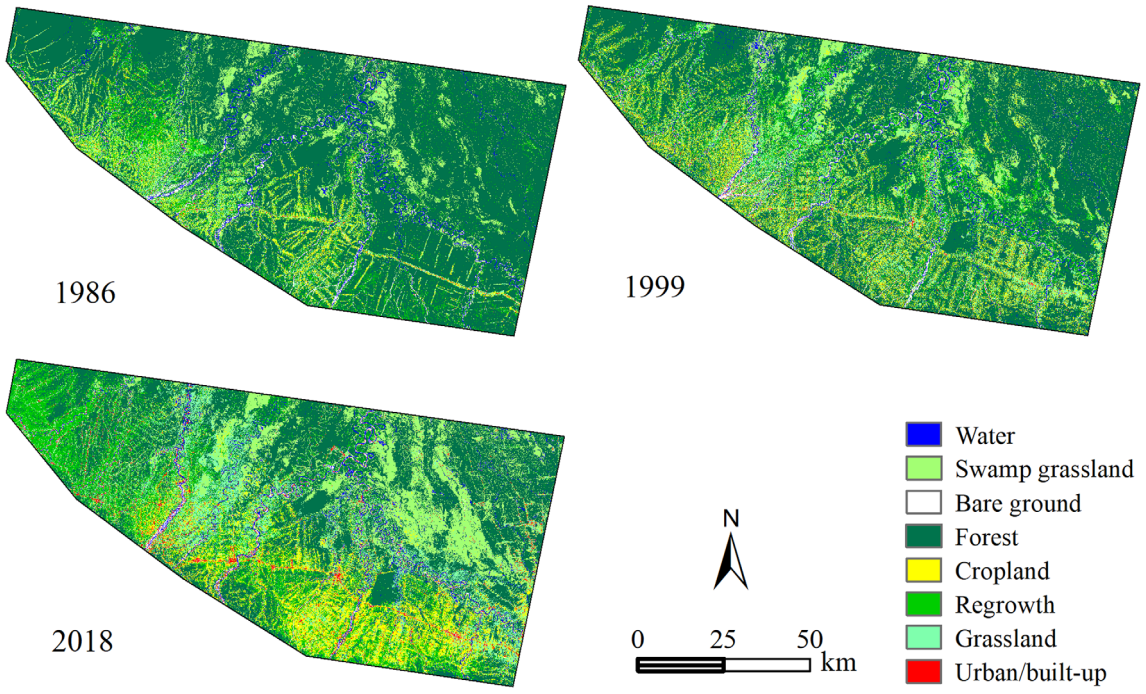

(a) Land cover maps for 1986, 1999, and 2018.

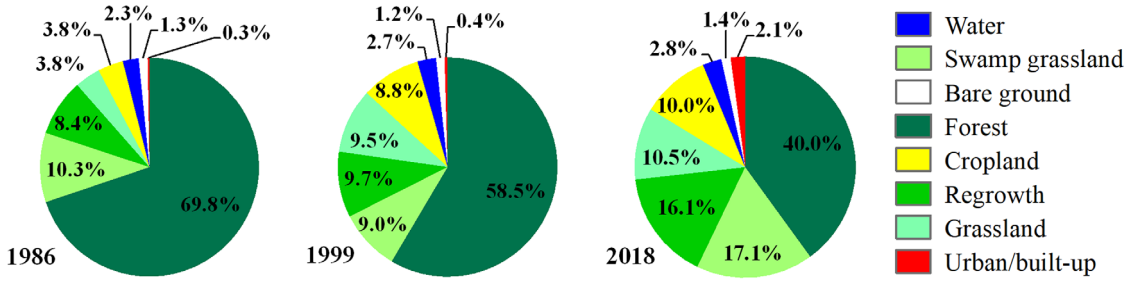

(b) Percentages of each land cover class in 1986, 1999, and 2018.

FIGURE 4 (a) Land-cover classification maps for 1986, 1999, and 2018 after merging land-cover categories (see Section 3.2 in text); (b) The percentages of the study area covered by each land-cover class in 1986, 1999, and 2018 [Colour figure can be viewed at wileyonlinelibrary.com]

TABLE 3 Percentage cover of merged land-cover classes for the study area in 1986, 1999, and 2018

Class	1986 (%)	1999 (%)	2018 (%)	Change in % 1986–1999	Change in % 1999–2018	Change in % 1986–2018
1. Water	2.34	2.74	2.77	0.40	0.03	0.43
2. Swamp grassland	10.27	9.05	17.15	−1.22	8.10	6.88
3. Bare ground	1.31	1.25	1.36	−0.07	0.11	0.05
4. Forest	69.81	58.50	39.99	−11.31	−18.51	−29.83
5. Cropland	3.77	8.76	10.03	4.99	1.26	6.25
6. Regrowth	8.44	9.71	16.07	1.27	6.37	7.64
7. Grassland	3.78	9.54	10.52	5.77	0.98	6.75
8. Urban/built-up	0.28	0.45	2.11	0.17	1.67	1.84

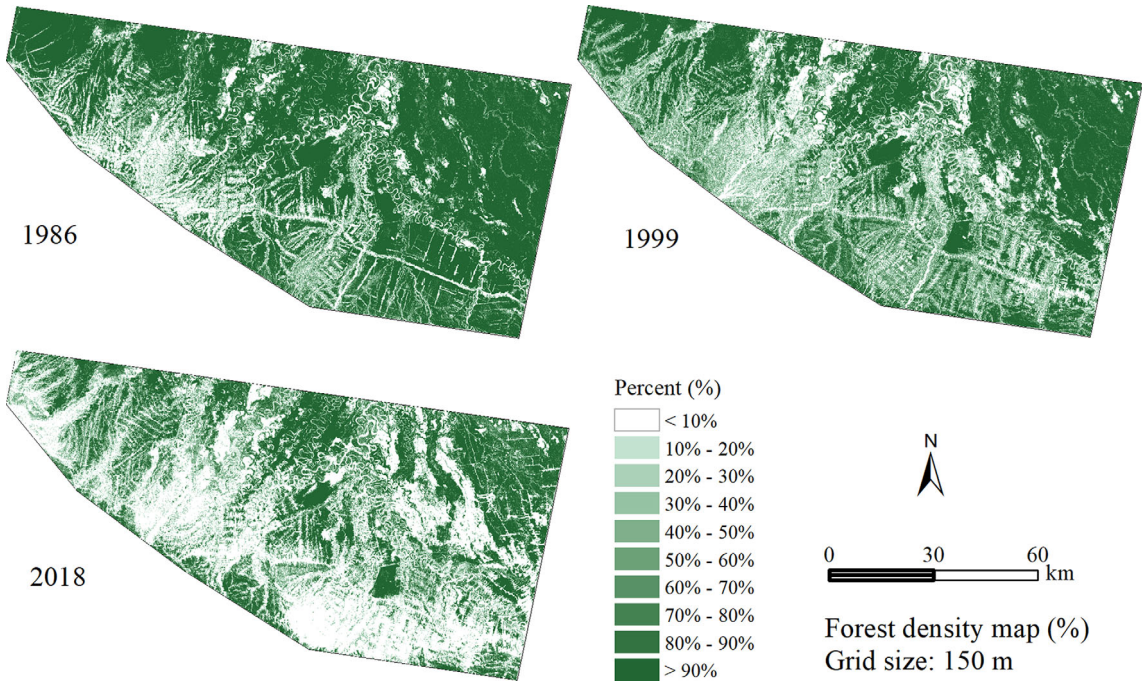

FIGURE 5 Comparison of the spatial distribution of forest percentage in each grid-cell at the 150-m grid scale from 1986 to 2018 [Colour figure can be viewed at wileyonlinelibrary.com]

The development of the pattern of urban/built-up and bare ground over time in Figure 4 are consistent with the typical fishbone pattern of road network and agricultural settlement growth which is known to lead to forest fragmentation in the Amazon Basin. In the Chapare region, small agricultural fields have been cleared adjacent to feeder roads as they penetrated further into the remaining forest between 1986 and 2018. The last 19 years have witnessed an acceleration in the trend of constructing roads in previously unutilized forests, with pastureland and cropland replacing forests. Figure 4 shows that cropland and grassland areas have expanded rapidly in this period. This has been accompanied by a marked decrease in forest area over the period 1986–2018 indicating an increase in the overall forest clearance rate, which in turn is related to the relatively low increase in regrowth between 1986 and 1999, compared to the period after 1999.

4.2 | Analysis of land-cover change trajectories

We calculated forest density at 150-m scale grid-cell for 1986, 1999, and 2018 (Figure 5).

To reveal spatiotemporal changes in forest density, we calculated the percentage changes in forest cover at the 150 m scale for 1986–1999 and 1999–2018 (Figure S2). The value for each grid-cell for each time interval was calculated by subtracting the forest area in 1986 from that in 1999, and then 1999 from 2018. We then divided the changes in forest area by the cell area. There has been a trend of forest clearance across the entire study area from the early nucleus of settlements in central Chapare between 1986 and 2018. From 1986 to 1999 deforestation mainly occurred in southeastern and central Chapare, but after 1999 clearance had expanded to cover almost the entire study area (Figure S2).

The annual standardized deforestation rates (ρ) were 1.36% for 1986–1999 and 2.0% for 1999–2018: forest was lost more slowly between 1986 and 1999 than between 1999 and 2018. Using the data in Table 3 we calculated the total amounts of forest cleared over the past three decades: 1075 km^2 of forest was cleared between 1986 and 1999 and a further 1,760 km^2 from 1999 to 2018. Most of the forest cleared in both time intervals was replaced by either grassland (mainly pasture for cattle grazing) or cropland.

We also calculated correlation coefficients between the land-cover changes for the two intervals (Table S1). These revealed that forest loss was negatively correlated with increases in swamp grassland (r = −.36), cropland (−.33), regrowth (−.43), and grassland (−.46) between 1986 and 1999.

We calculated changes in the spatial distribution of the percentage of forest cover for each grid-cell between 1986 and 2018 at the 150, 300, 600, and 900 m scales (Figure 6). The calculation for each grid-square cell value was described above (Section 3.2).

We extracted a subset in the west of the study area (Figure 1a, blue rectangle) to visualize the differences in the spatial patterns of land cover, forest density, and deforestation at the 150, 300, 600, and 900 m scales more clearly (Figure 7).

The number of fields between feeder roads dramatically increased as more forest was cleared for cultivation and grazing between 1986 and 2018, even though the road network did not alter much (Figure 7a,b). Figure 7c shows that forest clearance increased rapidly between 1999 and 2018. By comparing percentage changes in forest cover at 150, 300, 600, and 900 m grid scales for 1986–2018 (Figure 7c,d), it is clear that the 150 m grid extracted useful information about forest clearance more clearly than coarser-scale grid cells. We summarize the land-cover change correlations between 1986 and 2018 at the 150, 300, 600, and 900 m scales in Table S2. The changes in forest area are strongly negatively correlated with changes in cropland, regrowth, swamp grassland, and grassland at all four grid scales.

Although the correlation coefficients between the land-cover categories at all four-grid scales are similar (Table S2), 150-m grid cells extract deforestation structures more clearly than grid-cell scales of 300, 600, and 900 m (Figure 6). This, and the fact that the finer grid-cell scale revealed more spatial detail about deforestation, allows us to limit the discussion in the next section to the results obtained when using 150 m scale grids.

Finally, we prepared representative 2D density plots of changes in land-cover categories at the 900 m grid-cell scale between 1986

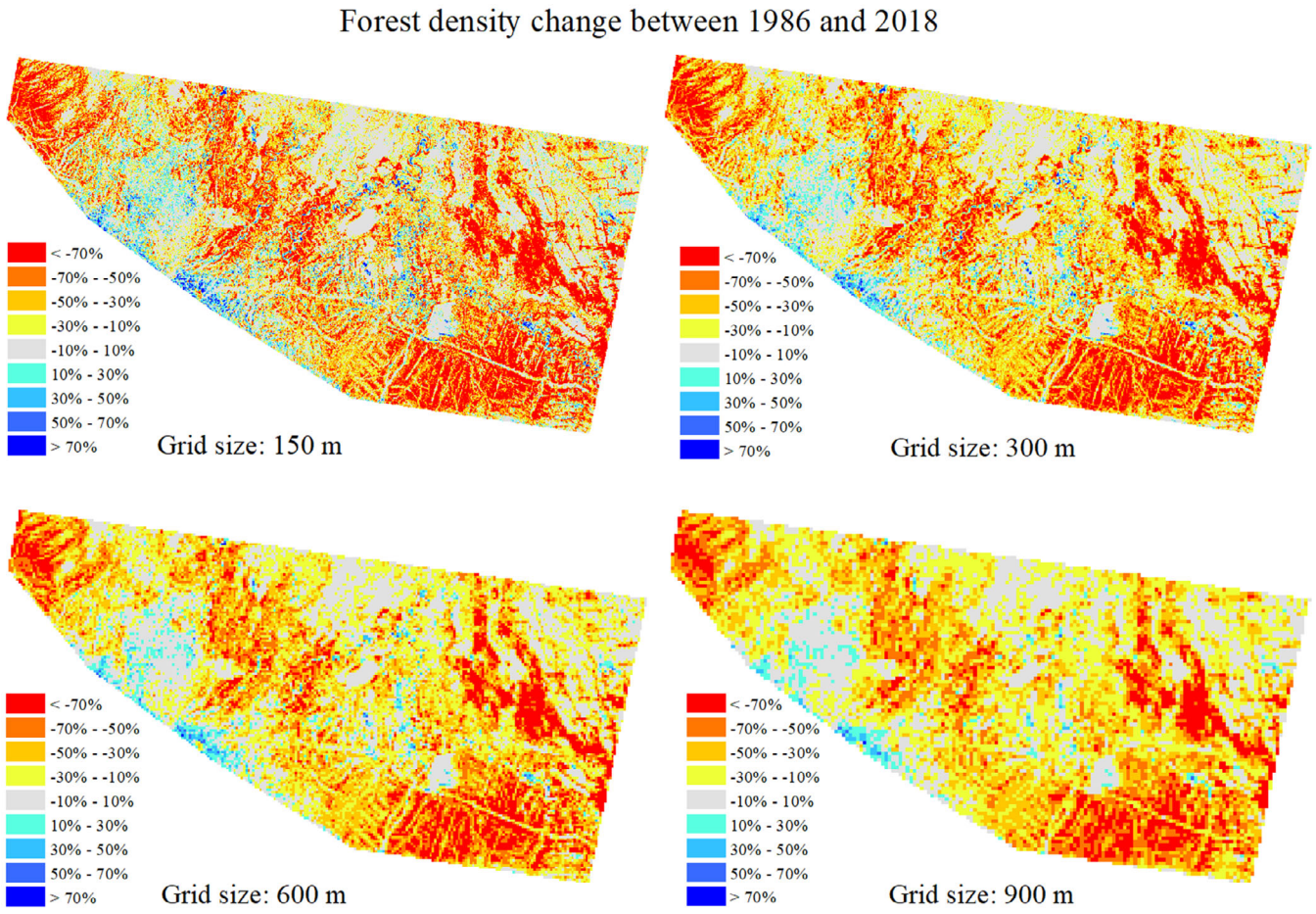

FIGURE 6 Comparison of the spatial distribution of the percent change in forest cover at 150, 300, 600, and 900 m grid scales from 1986 to 2018 [Colour figure can be viewed at wileyonlinelibrary.com]

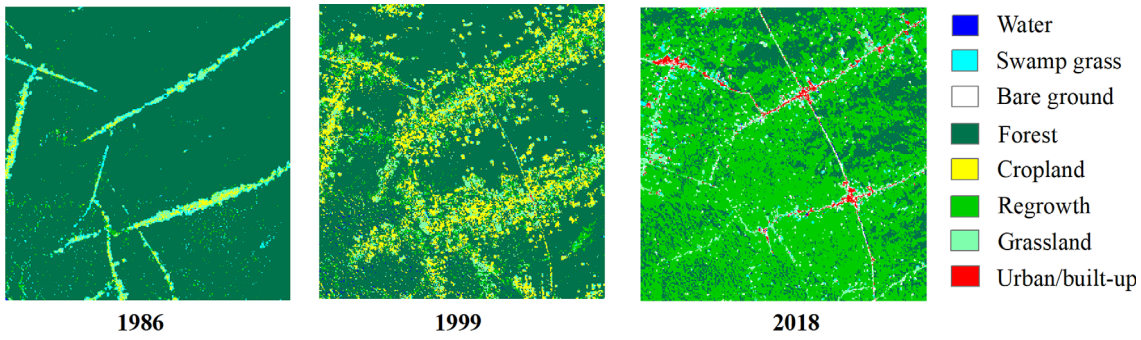

(a) Land cover maps for 1986, 1999, and 2018.

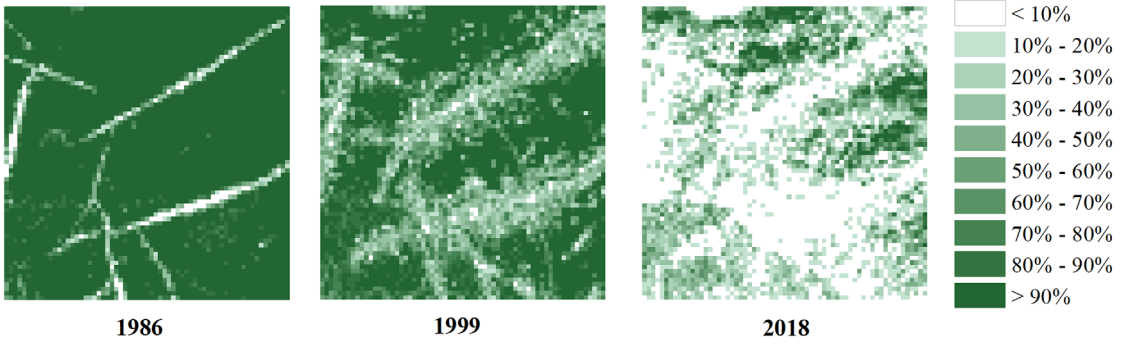

(b) Forest percentage density maps at the 150-m grid scale.

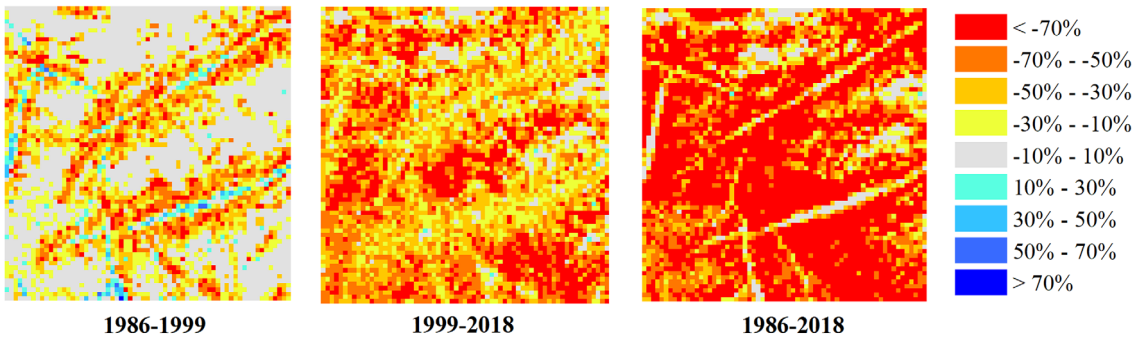

(c) Percentage change in forest cover at the 150-m grid scale.

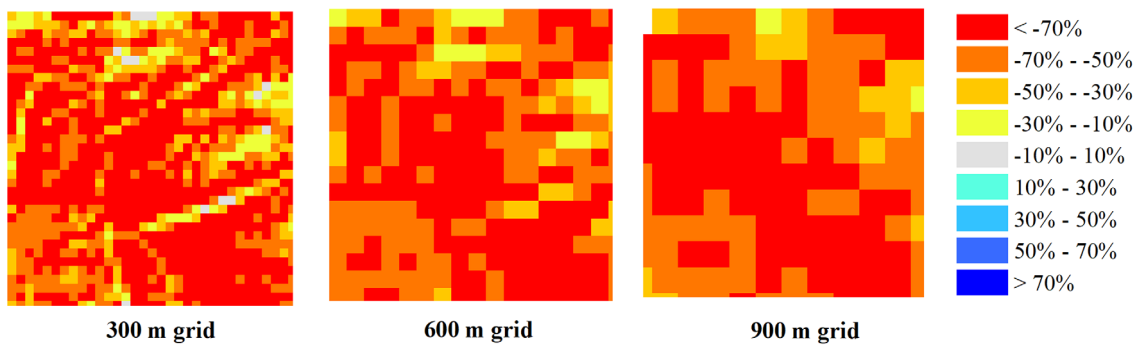

(d) Percentage change in forest cover at the 300, 600, and 900 m grid scales from 1986 to 2018.

FIGURE 7 (a) Comparison of the land-cover maps for 1986, 1999, and 2018; (b) Forest percentage at 150 m grid scales; (c) Percentage change in forest cover for 1986–1999, 1999–2018, and 1986–2018 at 150 m grid scales; (d) Percentage change in forest cover at 300, 600, and 900 m grid scales for 1986–2018. The area in each of these images is indicated by the blue rectangle in Figure 1a [Colour figure can be viewed at wileyonlinelibrary.com]

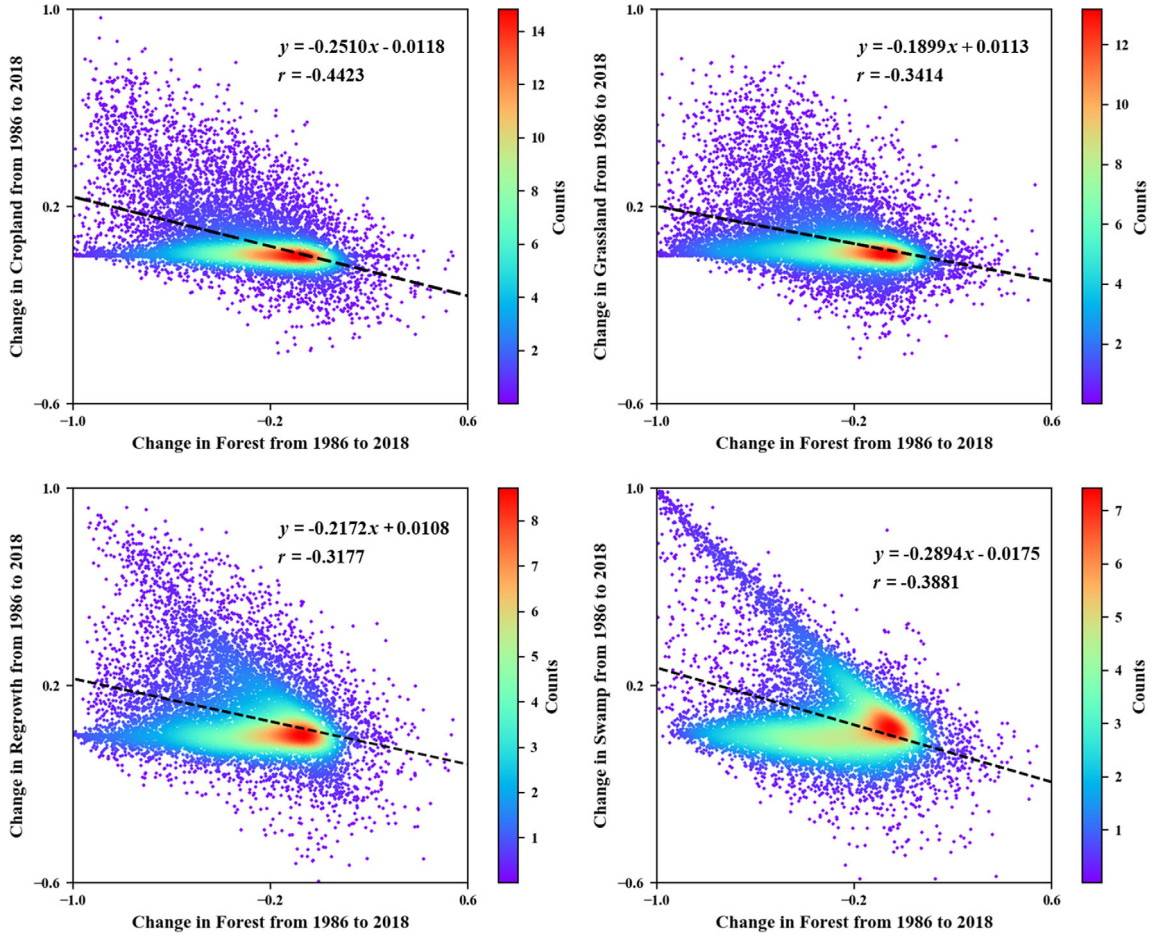

FIGURE 8 2D density plots (using Gaussian kernel density estimate) of percent change in land-cover categories during the study period at 900-m grid scale. The correlations were calculated using data for all 11,447 900-m scale grid-cells. Dashed lines and equations represent the results of linear regression analysis applied to all data [Colour figure can be viewed at wileyonlinelibrary.com]

and 2018 (Figure 8). These confirm that large areas of forest have been converted to cropland, grassland, and regrowth during the last three decades.

Grid cell-based land-cover change trajectories analysis enabled land-cover maps to be linked unambiguously and therefore provided reliable information on land-cover change for the same areas. This is an improvement in comparisons made between pixel-based comparisons, and provides a high level of confidence in the results.

5 | DISCUSSION

The discussion focuses initially on broad trends in land-cover change in the Chapare region, before analyzing the land-cover changes that have taken place through inferences drawn from spatial patterns and quantitative analyses. Given that Chapare is a globally important coca source region, the ability to determine the direct and indirect effects of coca cultivation on deforestation from this research is analyzed. Finally, key environmental and methodological issues used are discussed.

In terms of the main land-use conversion trajectories, change detection analysis revealed that 435.9 and 363.1 km^2 of forest were converted to grassland (pasture) and cropland between 1986 and 1999, respectively (Figure S2). While between 1999 and 2018, 397.2 and 352.0 km^2 of forest were converted to grassland and cropland. These trends are consistent with other research from the Amazon Basin where in-migration, settlement, and agricultural expansion are key deforestation drivers (De Sy et al., 2015; Grinand et al., 2013). The parallel trends of declining forest cover and increasing amounts of cropland and pasture are intuitive for an area that has been colonized by migrants who have been encouraged to develop an agricultural frontier by the Bolivian Government.

The forest losses must be considered 'net' losses because some cleared areas may have regenerated to the stage of mature secondary forest in the two time frames considered, though our knowledge of the area suggests that these areas will be a relatively small. Both the net forest losses and the broad land-use changes mask the fact that forest has been replaced by a fine-grained mosaic of many different crops, pasture, and regrowth of various ages across Chapare in the last 32 years. This multiplicity of land-uses has resulted from

economic decisions made by individual farmers in response to various agricultural policies which have changed significantly over the time frame of the research. The fine grain of the resulting landscape is created by farmers being given long, narrow areas to farm, and the fact that these areas are then divided into many fields over time (Bradley & Millington, 2008a; Bradley & Millington, 2008b). From the remote sensing point-of-view large tracts of terrestrial or swamp forest, which are relatively spectrally homogenous at the spatial resolutions of LANDSAT series sensors, have been replaced a far more spectrally heterogeneous landscape.

While the rates of forest conversion were rather higher after 1999; the rates of increase in the cropland and grassland were similar before and after 1999 (Table 3). This suggests the loss of forest to cropland and grassland is not a straightforward process and requires further investigation. It was not possible to validate these apparently constant increases in cropland and pasture areas over the 1986–2018 time frame for Chapare with an independent data set, as the highly detailed third national agricultural census in 2013 (Estado Plurionacional de Bolivia, , 2015) cannot be compared to the much less detailed 1984 agricultural census with any clarity.

As the increases in cropland and grassland (pasture) have followed similar trajectories since 1986, the cropland-pasture mix must have remained more-or-less the same across the region. This also means that cropland-pasture mix in central and southeastern Chapare that existed before 1999 has been replicated as the remaining forest in central and southeastern Chapare has been cleared; and as the main thrust of settlement and clearance shifted northwestwards after 1999. Interestingly this has occurred despite environmental differences, particularly soil properties and hydrological conditions, that exist across the area.

As intimated earlier, it is not possible to discuss forest conversion in Chapare without considering the role of coca. Given the fact that the cropland-pasture mix has remained more-or-less the same since 1986, it might be concluded that coca has had little influence on forest conversion. However, as the amounts of coca grown have varied significantly over the 32 years studied (UNODC, 2019, and UNODC reports from 2005 to 2018), as has the effectiveness of implementing anti-narcotic policies (Bradley & Millington, 2008a), that might be a false conclusion. The research we conducted did not enable us to determine any direct effects of coca on forest conversion in Chapare. This was due to the fact that: (a) individual land parcels of different crops cannot be determined with Landsat series data due to the spectral similarities of many crops and the small areas of cultivation; (b) the contributions of very small coca fields (Kaimowitz, 1997) to the overall cropland pattern are marginal compared to the total cultivated area; and (c) the fact that farmers switch between coca and other field crops with relative ease. UNODC have used fine-spatial resolution imagery acquired by spaceborne and airborne sensors since 2004 in coca monitoring, but the results are limited in terms of determining land-use trajectories. Moreover, it is not possible to undertake such analysis back to the 'coca boom' because fine-scale, multispectral imagery is unavailable for the 1970s and 1980s.

Hoffman et al., (Hoffmann et al., 2018) suggest the indirect effects of coca cultivation on forest loss are probably greater than direct effects. Coca is a frequent component of the land-use mix in areas of new colonization on the peripheries of the cultivated zone in Chapare (Bradley & Millington, 2008a). In such locations it has been often grown with less surveillance than other parts of Chapare in these areas. To provide an initial test of this imagery from a peripheral area in northwest Chapare, where our field observations have recorded pioneer settlements with a land-use mosaic of large tracts of uncleared forest, very small areas of cropland (mostly coca fields), and intermediate amounts of pasture is provided in Figure S3.

The 1986 maps show that settlers had used geophysical surveys lines cut through primary forest as lines of access to settle in the area and create farms. By this time, the cropland and grassland areas had not encroached far into the primary forest. We do not have contemporary field data from this area, but Bradley and Millington (2008a) show that farms in similar, early stages of settlement in central Chapare often had coca as part of their crop mix. Farmers then cleared back from the tracks to create longer farms with more cropland and pasture. More extensive clearance with increased areas of pasture and cropland, and less primary forest, is clear in the 1999 and 2018 images. Field surveys conducted in this area (August 2007 and September 2015) indicate that grazing and coca cultivation dominate post-clearance land uses in the region covered by Figure S3. However, any arguments that can be made about the indirect (or direct) roles of coca in this area cannot be based on remotely sensed data alone: it requires both field observations and an understanding of the geographical context. We conclude that it is not possible to unambiguously map the indirect effects of coca on deforestation in Chapare using time sequence of LANDSAT data alone.

What then can we deduce about the drivers of deforestation in this region from this remote sensing and GIS analysis? The evidence presented in Figure 7 signals the important role of road building in fragmenting forests that has been noted by other researchers (Davidson et al., 2012; Dissanayake et al., 2019). We can infer from this that the fishbone forest clearance pattern (Figure 5), which has been observed frequently in the Amazon Basin (de Filho & Metzger, 2006; Ewers & Laurance, 2006) is present. This was noted earlier in central and southeastern Chapare (Millington et al., 2003) and analyzed in the lowlands of Carrasco Province (southeast Chapare) by van Gils and Loza Armand Ugon (2006). Applying Bradley and Millington's (2008b) theoretical model of forest fragmentation to the spatial patterns of forest fragmentation shown in this article, confirms that the fishbone pattern arises from a combination of road building and government land grants along the roads throughout Chapare. We argue that an integrated road-land grant driver of deforestation should be considered in areas like Chapare where there has been very little spontaneous colonization of forested areas in the time frame of this research. The introduction of such an integrated driver into the land-use/land-cover change literature would provide a mechanism to support Fernández-Llamazares et al.'s (2018) finding that the extension of road networks increases deforestation rates.

The percentages of cropland and grassland in Chapare increased by factors of 2.6 and 2.8 between 1986 and 2018, respectively (Table 3 and Figure 4b). While metrics like these provide headline figures, caution should be exercised in applying them across large areas. In the case of Chapare the increases in the proportions of cropland and grassland to 1999 can only be applied to central and southeastern Chapare with any certainty. While after 1999, they can be applied more broadly to the region. However, even after 1999 an issue arises because the forest clearance, cultivation, and pastoral, frontiers were mainly in northwestern and the remoter parts of central and southeastern Chapare. It is worthwhile noting that the deforestation rates and net forest losses obtained from this study are higher than the average deforestation rate of 1% for Bolivia (Armenteras, María, Rodríguez, & Retana, 2017) and the country's net loss of forest area (FAO, 2015).

The correlations between the changes in land-cover categories over the two time periods studied lend support to these arguments in that forest losses are negatively correlated with increases in cropland and grassland. Correlation coefficients of forest loss and increases in cropland were slightly weaker in 1999–2018 (r = −.27) compared to 1986–1999 (r = −.33), while those between forest losses and grassland were much stronger for 1986–1999 (r = −.46) than for 1999–2018 (r = −.21; Table S1). However, the lower correlation coefficients of forest-cropland and forest-pasture conversion in the second time period do not readily lend support to the fact that the cropland-pasture balance has changed little since 1986. The relationships between cropland and regrowth, and grassland and regrowth, are potentially important in explaining this. Cropland-regrowth dynamics are of particular importance because many of the annual crops in the region are grown under a slash-and-burn systems—the intensity of which varies with population and cultivation densities; and the amount of alternative crops grown during periods when anti-narcotic policies were enforced, particularly in the 1990s. This also applies to some other crops which are grown for only a few years before fields are abandoned, for example, pineapples and heart of palm. Between 1986 and 1999, 26.0 km^2 of cropland reverted to regrowth, while from 1999 to 2018 this rose to 213.0 km^2, which may be due to more fields being left to fallow in central and southeastern Chapare before 1999 when there was a relatively large pool of primary forest. However, as more people have migrated to the Chapare, land has become scarcer (pers. comm. Susanna Arrazola, Centro de Biodiversidad y Genética, Universidad Mayor San Simon, Cochabamba). Land grants have become smaller and farmers cannot afford large proportions of their farms to remain as fallow regrowth. That, along with the more permanent cultivation patterns that now exist in central and southeastern Chapare, will have reduced the proportion of cultivable land that can be under fallow regrowth. It is worthwhile noting that the results from the quantitative analysis obtained using the grid-cell-based approach could not easily have been generated in pixel-based analysis. Although the results obtained at the finer grid-cell scale of 150 m revealed more spatial detail about deforestation, the relationship between grid-cell scale and quantitative analysis is unclear and requires further investigation.

In terms of environmental outcomes, the replacement of tropical forest with agriculture accentuates flooding and soil erosion (Souza-Filho et al., 2016). This will be the case in Chapare (Torrico, Pohlan, & Janssens, 2005) and will particularly affect the newer farming settlements that are already susceptible to seasonal flooding in the north of Chapare. Local microclimates have already been impacted by the replacement of forest with grasses, annual and perennial crops. In addition to this local effect, carbon emissions associated with the land-use changes and a reduction in carbon sequestration capacity, will have contributed to climate change globally (Marques et al., 2019). Land-cover change can also have additional biophysical effects, such as local temperature changes (Duveiller et al., 2020). The new agroecosystems created will also have impacted directly on biodiversity in the region. Therefore, routine application of the techniques outlined in this research is necessary if Bolivia is to manage the ecosystem services that Chapare provides.

The subspace method used classified the image data into several classes based on a set of class subspaces, which were generated from a set of training samples of each class using principal component analysis. One of the main stated advantages of subspace over other classification methods is that continual updating of the class covariance matrices reduces the overlap between class subspaces in the learning phase of the procedure. While this provided clarity for most classes, we noticed that discrimination between the urban/built-up and bare ground classes was still limited, as it was to a lesser extent for forest and regrowth. This is due to the similar spectral characteristics between the pairs of classes in both cases (Figure S1). These issues are potentially problematic in understanding land-use dynamics in the region because the bare ground class represents areas of soil which are being cultivated and highly degraded pasture, and needs to be differentiated from urban expansion and other changes to infrastructure. In the case of forest and regrowth created some of the issues around interpreting the role of regrowth in understanding forest-cropland dynamics. These problems are unlikely to be resolved with visible and shortwave infrared data, and future research should combine optical and synthetic aperture radar remote sensing data to improve the between discrimination of urban/built-up and bare ground classes, or extend the subspace method by adopting a nonlinear transformation defined by kernel functions (Park & Konishi, 2019).

6 | CONCLUSIONS

The 32 years from 1986 to 2018 witnessed an acceleration in the transformation of natural forests to a fine-grained mosaic of cultivation and grazing, secondary forest regrowth, forest remnants, and agricultural settlements in Chapare: a process began in the late 1950s and early 1960s.

Almost a third of the forest that remained in 1986 (2,835 ha) had been lost by 2018. Forest clearance has accelerated since 1986, with mean annual deforestation rates increasing from 1.36% (1986–1999) to 2.0% after 1999. In addition, the locus of deforestation has shifted from central and southeastern Chapare to the northwest. The

deforestation rates and net forest losses in Chapare are higher than the average deforestation rate, and the net loss of forest area, for Bolivia. The main drivers of tropical forest conversion in the region have been in-migration, settlement, and agricultural expansion. We suggest that government-led development of the road network, which is very closely tied to government land grants to farmers, should be combined into a road-land grant driver. However, we were unable to identify either direct or indirect effects of coca on forest loss in the region. The net outcome of all deforestation drivers in the area has been that natural forested landscapes have been replaced by a highly altered fine-grained anthropic landscape driven by an expanding agricultural frontiers.

This study is applicable to discussions about potential future anthropogenic land-cover changes in other tropical forest areas. It provides insights that may be useful for informing policy and land-use planning, and accounting for the spatial and temporal dynamics of land-change trajectories in trying to achieve development and conservation targets.

ACKNOWLEDGMENTS

H.B. was supported by NSFC Grant No. 41771372 and a Mawson Lakes Research Fellowship to conduct research at Flinders University. A.M. was supported by grants from the Texas Agricultural Experiment Station (Texas A&M University) and the Flinders University Outside Studies Program. The 2003 field campaign was supported by an EU Framework IV grant under the INCO program, and the UK National Environmental Research Council. We acknowledge field assistance provided by Andrew Bradley, Mauricio Galloliendo, Felix Huanca, Lucho Ramirez, and Daniel Redo.

CONFLICT OF INTEREST

None.

ORCID

Hasi Bagan https://orcid.org/0000-0002-0471-7135

REFERENCES

Abdi, A. M. (2019). Land cover and land use classification performance of machine learning algorithms in a boreal landscape using Sentinel-2 data. *GIScience & Remote Sensing*, *57*, 1–20. https://doi.org/10.1080/15481603.2019.1650447

Achard, F., Beuchle, R., Mayaux, P., Stibig, H. J., Bodart, C., Brink, A., … Lupi, A. (2014). Determination of tropical deforestation rates and related carbon losses from 1990 to 2010. *Global Change Biology*, *20*(8), 2540–2554. https://doi.org/10.1111/gcb.12605

Armenteras, D., María, J., Rodríguez, N., & Retana, J. (2017). Deforestation dynamics and drivers in different forest types in Latin America: Three decades of studies (1980–2010). *Global Environmental Change*, *46*, 139–147. https://doi.org/10.1016/j.gloenvcha.2017.09.002

Awotwi, A., Anornu, G. K., Quaye-Ballard, J. A., & Annor, T. (2018). Monitoring land use and land cover changes due to extensive gold mining, urban expansion, and agriculture in the Pra River Basin of Ghana, 1986–2025. *Land Degradation & Development*, *29*(10), 3331–3343. https://doi.org/10.1002/ldr.3093

Bagan, H., & Yamagata, Y. (2010). Improved subspace classification method for multispectral remote sensing image classification. *Photogrammetric Engineering and Remote Sensing*, *76*(11), 1239–1251. https://doi.org/10.14358/PERS.76.11.1239

Bagan, H., & Yamagata, Y. (2012). Landsat analysis of urban growth: How Tokyo became the world's largest megacity during the last 40 years. *Remote Sensing of Environment*, *127*, 210–222. https://doi.org/10.1016/j.rse.2012.09.011

Bagan, H., & Yamagata, Y. (2014). Land-cover change analysis in 50 global cities by using a combination of Landsat data and analysis of grid cells. *Environmental Research Letters*, *9*(6), 064015. https://doi.org/10.1088/1748-9326/9/6/064015

Bagan, H., Kinoshita, T., & Yamagata, Y. (2012). Combination of AVNIR-2, PALSAR, and polarimetric parameters for land cover classification. *IEEE Transactions on Geoscience and Remote Sensing*, *50*(4), 1318–1328. https://doi.org/10.1109/TGRS.2011.2164806

Batunacun, N., Hu, Y., & Lakes, T. (2018). Land-use change and land degradation on the Mongolian Plateau from 1975 to 2015—A case-study from Xilingol, China. *Land Degradation & Development*, *29*(6), 1595–1606. https://doi.org/10.1002/ldr.2948

Bottazzi, P., & Dao, H. (2013). On the road through the Bolivian Amazon: A multi-level land governance analysis of deforestation. *Land Use Policy*, *30*, 137–146. https://doi.org/10.1016/j.landusepol.2012.03.010

Bovolo, C. I., & Donoghue, D. (2017). Has regional forest loss been underestimated? *Environmental Research Letters*, *12*(11), 111003. https://doi.org/10.1088/1748-9326/aa9268

Bradley, A., & Millington, A. (2008a). Coca and colonists: Quantifying and explaining forest clearance under coca and anti-narcotics policy regimes. *Ecology and Society*, *13*(1), 31. http://dx.doi.org/10.5751/es-02435-130131

Bradley, A., & Millington, A. (2008b). Developing a thick understanding of Forest fragmentation in landscapes of colonisation in the Amazon Basin. In R. J. Aspinall & M. J. Hill (Eds.), *Land use change. Science, policy and management* (pp. 119–137). Routledge: London.

Congalton, R. G., & Green, K. (2008). *Assessing the accuracy of remotely sensed data: Principles and practices*. Hoboken, NJ: Taylor & Francis Ltd.

Dávalos, L. M., Bejarano, A. C., Hall, M. A., Correa, H. L., Corthals, A., & Espejo, O. J. (2011). Forests and drugs: Coca-driven deforestation in tropical biodiversity hotspots. *Environmental Science & Technology*, *45*(4), 1219–1227. https://doi.org/10.1021/es102373d

Davidson, E. A., de Araújo, A. C., Artaxo, P., Balch, J. K., Brown, I. F., Bustamante, M. M., … Munger, J. W. (2012). The Amazon basin in transition. *Nature*, *481*(7381), 321. https://doi.org/10.1038/nature10717

de Filho, F. J. B. O., & Metzger, J. P. (2006). Thresholds in landscape structure for three common deforestation patterns in the Brazilian Amazon. *Landscape Ecology*, *21*(7), 1061–1073. https://doi.org/10.1007/s10980-006-6913-0

De Sy, V., Herold, M., Achard, F., Beuchle, R., Clevers, J. G. P. W., Lindquist, E., & Verchot, L. (2015). Land use patterns and related carbon losses following deforestation in South America. *Environmental Research Letters*, *10*(12), 124004. https://doi.org/10.1088/1748-9326/10/12/124004

Delgado, A. C. (2017). The TIPNIS conflict in Bolivia. *Contexto Internacional*, *39*(2), 373–392. https://doi.org/10.1590/S0102-8529.2017390200009

Dissanayake, D. M. N. J., Zhai, D. L., Dossa, G. G. O., Shi, J., Luo, Q., & Xu, J. (2019). Roads as drivers of above-ground biomass loss at tropical forest edges in Xishuangbanna, Southwest China. *Land Degradation & Development*, *30*(11), 1325–1335. https://doi.org/10.1002/ldr.3316

Duveiller, G., Caporaso, L., Abad-Viñas, R., Perugini, L., Grassi, G., Arneth, A., & Cescatti, A. (2020). Local biophysical effects of land use and land cover change: Towards an assessment tool for policy makers. *Land Use Policy*, *91*, 104382. https://doi.org/10.1016/j.landusepol.2019.104382

Duveiller, G., Defourny, P., Desclée, B., & Mayaux, P. (2008). Deforestation in Central Africa: Estimates at regional, national and landscape levels by advanced processing of systematically-distributed Landsat extracts. *Remote Sensing of Environment*, *112*(5), 1969–1981. https://doi.org/10.1016/j.rse.2007.07.026

Estado Plurinacional de Bolivia. (2015). *Censo Agropecuario 2013*. La Paz: Instituto Nacional de Estadistica.

Ewers, R. M., & Laurance, W. F. (2006). Scale-dependent patterns of deforestation in the Brazilian Amazon. *Environmental Conservation*, *33*(3), 203–211. https://doi.org/10.1017/S0376892906003250

FAO. (2015). Global Forest Resources Assessment 2015. Desk Reference. Retrieved from http://www.fao.org/3/a-i4808e.pdf

Farthing, N., & Kohl, B. (2010). Social control: Bolivia;s new approach to coca reduction. *Latin American Perspectives*, *37*(4), 197–213. https://doi.org/10.1177/0094582X10372516

Fernández-Llamazares, Á., Helle, J., Eklund, J., Balmford, A., Moraes, R. M., Reyes-García, V., & Cabeza, M. (2018). New law puts Bolivian biodiversity hotspot on road to deforestation. *Current Biology*, *28*(1), R15–R16. https://doi.org/10.1016/j.cub.2017.11.013

Fukui, K., & Maki, A. (2015). Difference subspace and its generalization for subspace-based methods. *IEEE Transactions on Pattern Analysis and Machine Intelligence*, *37*(11), 2164–2177. https://doi.org/10.1109/TPAMI.2015.2408358

Godoy, R., Morduch, J., & Bravo, D. (1998). Technological adoption in rural Cochabamba, Bolivia. *Journal of Anthropological Research*, *54*(3), 351–372. https://doi.org/10.1086/jar.54.3.3630652

Grimmelmann, K., Espinoza, J., Arnold, J., & Arning, N. (2017). The land-drugs nexus: How illicit drug crop cultivation is related to access to land. *UNODC Bulletin on Narcotics: Alternative Development: Practices and Reflections*, *61*, 75–104. https://doi.org/10.18356/2a18d285-en

Grinand, C., Rakotomalala, F., Gond, V., Vaudry, R., Bernoux, M., & Vieilledent, G. (2013). Estimating deforestation in tropical humid and dry forests in Madagascar from 2000 to 2010 using multi-date Landsat satellite images and the random forests classifier. *Remote Sensing of Environment*, *139*, 68–80. https://doi.org/10.1016/j.rse.2013.07.008

Grisaffi, T., & Ledebur, K. (2016). Citizenship or repression? Coca, eradication and development in the Andes. *Stability: International Journal of Security and Development*, *5*(1), 1–19. http://doi.org/10.5334/sta.440

Hansen, M. C., Potapov, P. V., Moore, R., Hancher, M., Turubanova, S. A., Tyukavina, A., … Kommareddy, A. (2013). High-resolution global maps of 21st-century forest cover change. *Science*, *342*(6160), 850–853. https://doi.org/10.1126/science.1244693

Henkel, R. (1995). Coca (*Erythroxylum coca*) cultivation, cocaine production, and biodiversity loss in the Chapare region of Bolivia. In S. P. Churchill (Ed.), *Biodiversity and Conservation of Neotropical Montane Forests* (pp. 551–560). Bronx: The New York Botanical Garden.

Hoffmann, C., Márquez, J. R. G., & Krueger, T. (2018). A local perspective on drivers and measures to slow deforestation in the Andean-Amazonian foothills of Colombia. *Land Use Policy*, *77*, 379–391. https://doi.org/10.1016/j.landusepol.2018.04.043

Hussain, M., Chen, D., Cheng, A., Wei, H., & Stanley, D. (2013). Change detection from remotely sensed images: From pixel-based to object-based approaches. *ISPRS Journal of Photogrammetry and Remote Sensing*, *80*, 91–106. https://doi.org/10.1016/j.isprsjprs.2013.03.006

Kaimowitz, D. (1997). Factors determining low deforestation: The Bolivian Amazon. *Ambio*, *26*(8), 537–540.

Keenan, R. J., Reams, G. A., Achard, F., de Freitas, J. V., Grainger, A., & Lindquist, E. (2015). Dynamics of global forest area: Results from the FAO Global Forest Resources Assessment 2015. *Forest Ecology and Management*, *352*, 9–20. https://doi.org/10.1016/j.foreco.2015.06.014

Kiang, M. Y. (2003). A comparative assessment of classification methods. *Decision Support Systems*, *35*(4), 441–454. https://doi.org/10.1016/S0167-9236(02)00110-0

Killeen, T. J., Calderon, V., Soria, L., Quezada, B., Steininger, M. K., Harper, G., … Tucker, C. J. (2007). Thirty years of land-cover change in Bolivia. *Ambio*, *36*(7), 600–607. https://doi.org/10.1579/0044-7447(2007)36[600:TYOLCI]2.0.CO;2

Killeen, T. J., Guerra, A., Calzada, M., Correa, L., Calderon, V., Soria, L., … Steininger, M. K. (2008). Total historical land-use change in eastern Bolivia: Who, where, when, and how much? *Ecology and Society*, *13*(1), 36. https://doi.org/10.5751/ES-02453-130136

Kohl, B., & Breshahan, R. (2010). Bolivia under morales: Consolidating power, initiating decolonization. *Latin American Perspectives*, *37*(3), 5–17. https://doi.org/10.1177/0094582X10364030

Lima, L. S., Coe, M. T., Soares Filho, B. S., Cuadra, S. V., Dias, L. C., Costa, M. H., … Rodrigues, H. O. (2014). Feedbacks between deforestation, climate, and hydrology in the Southwestern Amazon: Implications for the provision of ecosystem services. *Landscape Ecology*, *29*(2), 261–274. https://doi.org/10.1007/s10980-013-9962-1

Lu, D., Batistella, M., Mausel, P., & Moran, E. (2007). Mapping and monitoring land degradation risks in the Western Brazilian Amazon using multitemporal Landsat TM/ETM+ images. *Land Degradation & Development*, *18*(1), 41–54. https://doi.org/10.1002/ldr.762

Malingreau, J. P., Eva, H. D., & De Miranda, E. E. (2012). Brazilian Amazon: A significant five year drop in deforestation rates but figures are on the rise again. *Ambio*, *41*(3), 309–314. https://doi.org/10.1007/s13280-011-0196-7

Marengo, J. A., Souza, C. A., Thonicke, K., Burton, C., Halladay, K., Betts, R., & Soares, W. R. (2018). Changes in climate and land use over the Amazon Region: Current and future variability and trends. *Frontiers in Earth Science*, *6*, 228. https://doi.org/10.3389/feart.2018.00228

Marques, A., Martins, I. S., Kastner, T., Plutzar, C., Theurl, M. C., Eisenmenger, N., … Canelas, J. (2019). Increasing impacts of land use on biodiversity and carbon sequestration driven by population and economic growth. *Nature Ecology & Evolution*, *3*(4), 628–637. https://doi.org/10.1038/s41559-019-0824-3

Millington, A. C. (2018). Creating coca frontiers and cocaleros in Chapare: Bolivia, 1940 to 1990. In *The origins of cocaine* (pp. 96–125). New York: Routledge, Taylor and Francis Group.

Millington, A. C., Velez-Liendo, X. M., & Bradley, A. V. (2003). Scale dependence in multitemporal mapping of forest fragmentation in Bolivia: Implications for explaining temporal trends in landscape ecology and applications to biodiversity conservation. *ISPRS Journal of Photogrammetry and Remote Sensing*, *57*(4), 289–299. https://doi.org/10.1016/S0924-2716(02)00154-5

Montes de Oca, I. (1997). *Geografía y Recursos Naturales de Bolivia* (3rd ed.). La Paz, Bolivia: EDOBOL.

Morales, W. Q. (2013). The TIPNIS crisis and the meaning of Bolivian democracy under Evo Morales. *The Latin Americanist*, *57*(1), 79–90. https://doi.org/10.1111/j.1557-203X.2012.01186.x

Müller, R., Pacheco, P., & Montero, J. C. (2014). *The context of deforestation and forest degradation in Bolivia*. Bogor, Indonesia: Center for International Forestry Research.

Oja, E. (1983). *Subspace methods of pattern recognition*. Letchworth, UK: Research Studies Press and John Wiley & Sons.

Ometto, J. P., Aguiar, A. P. D., & Martinelli, L. A. (2011). Amazon deforestation in Brazil: Effects, drivers and challenges. *Carbon Management*, *2*(5), 575–585. https://doi.org/10.4155/cmt.11.48

Paneque-Gálvez, J., Mas, J. F., Guèze, M., Luz, A. C., Macía, M. J., Orta-Martínez, M., … Reyes-García, V. (2013). Land tenure and forest cover change. The case of southwestern Beni, Bolivian Amazon, 1986–2009. *Applied Geography*, *43*, 113–126. https://doi.org/10.1016/j.apgeog.2013.06.005

Paneque-Gálvez, J., Pérez-Llorente, I., Luz, A. C., Guèze, M., Mas, J. F., Macía, M. J., … Reyes-García, V. (2018). High overlap between traditional ecological knowledge and forest conservation found in the Bolivian Amazon. *Ambio*, *47*(8), 908–923. https://doi.org/10.1007/s13280-018-1040-0

Park, H., & Konishi, S. (2019). Sparse kernel subspace method for classifying and representing patterns from data with complex structure. *Communications in Statistics-Simulation and Computation*, 1–17. https://doi.org/10.1080/03610918.2019.1620271

Pinto-Ledezma, J. N., & Mamani, M. L. R. (2014). Temporal patterns of deforestation and fragmentation in lowland Bolivia: Implications for climate change. *Climatic Change*, *127*, 43–54. https://doi.org/10.1007/s10584-013-0817-1

Puyravaud, J. P. (2003). Standardizing the calculation of the annual rate of deforestation. *Forest Ecology and Management*, *177*(1–3), 593–596. https://doi.org/10.1016/S0378-1127(02)00335-3

Rodríguez Ostria, G. (1972). *Historia del Trópico Cochabambino*. Cochabamba: Prefectura del Departamento del Cocahabamba.

Shoman, W., Alganci, U., & Demirel, H. (2019). A comparative analysis of gridding systems for point-based land cover/use analysis. *Geocarto International*, *34*(8), 867–886. https://doi.org/10.1080/10106049.2018.1450449

Song, C., Woodcock, C. E., Seto, K. C., Lenney, M. P., & Macomber, S. A. (2001). Classification and change detection using Landsat TM data: When and how to correct atmospheric effects? *Remote Sensing of Environment*, *75*(2), 230–244. https://doi.org/10.1016/S0034-4257(00)00169-3

Souza-Filho, P. W. M., de Souza, E. B., Júnior, R. O. S., Nascimento, W. R., Jr., de Mendonça, B. R. V., Guimarães, J. T. F., … Siqueira, J. O. (2016). Four decades of land-cover, land-use and hydroclimatology changes in the Itacaiúnas River watershed, southeastern Amazon. *Journal of Environmental Management*, *167*, 175–184. https://doi.org/10.1016/j.jenvman.2015.11.039

Tejada, G., Dalla-Nora, E., Cordoba, D., Lafortezza, R., Ovando, A., Assis, T., & Aguiar, A. P. (2016). Deforestation scenarios for the Bolivian lowlands. *Environmental Research*, *144*, 49–63. https://doi.org/10.1016/j.envres.2015.10.010

Torrico, J. C., Pohlan, H. A. J., & Janssens, M. J. (2005). Alternatives for the transformation of drug production areas in the Chapare region, Bolivia. *Journal of Food Agriculture and Environment*, *3*(3/4), 167–172. https://doi.org/10.1234/4.2005.679

Tyukavina, A., Hansen, M. C., Potapov, P. V., Stehman, S. V., Smith-Rodriguez, K., Okpa, C., & Aguilar, R. (2017). Types and rates of forest disturbance in Brazilian legal Amazon, 2000–2013. *Science Advances*, *3*(4), e1601047. https://doi.org/10.1126/sciadv.1601047

UNODC. (2019). Estado Plurinacional de Bolivia. Monitereo de Cultivos de Coca 2018. UNODC, La Paz. 81p. Retrieved from https://www.unodc.org/documents/crop-monitoring/Bolivia/Bolivia_Informe_Monitoreo_Coca_2018_web.pdf

van Gils, H. A., & Ugon, A. V. L. A. (2006). What drives conversion of tropical forest in Carrasco Province, Bolivia? *Ambio*, *35*, 81–85. https://doi.org/10.1579/0044-7447(2006)35[81:WDCOTF]2.0.CO;2

Wulder, M. A., Loveland, T. R., Roy, D. P., Crawford, C. J., Masek, J. G., Woodcock, C. E., … Dwyer, J. (2019). Current status of Landsat program, science, and applications. *Remote Sensing of Environment*, *225*, 127–147. https://doi.org/10.1016/j.rse.2019.02.015

Yin, H., Prishchepov, A. V., Kuemmerle, T., Bleyhl, B., Buchner, J., & Radeloff, V. C. (2018). Mapping agricultural land abandonment from spatial and temporal segmentation of Landsat time series. *Remote Sensing of Environment*, *210*, 12–24. https://doi.org/10.1016/j.rse.2018.02.050

SUPPORTING INFORMATION

Additional supporting information may be found online in the Supporting Information section at the end of this article.

How to cite this article: Bagan H, Millington A, Takeuchi W, Yamagata Y. Spatiotemporal analysis of deforestation in the Chapare region of Bolivia using LANDSAT images. *Land Degrad Dev*. 2020;1–16. https://doi.org/10.1002/ldr.3692